Article

A Raman Microspectroscopy Study of Water and Trehalose in Spin-Dried Cells

Alireza Abazari,[1] Nilay Chakraborty,[2] Steven Hand,[3] Alptekin Aksan,[4] and Mehmet Toner[1,*]

[1]The Center for Engineering in Medicine, Massachusetts General Hospital, Harvard Medical School, and Shriners Hospital for Children, Boston, Massachusetts; [2]Department of Mechanical Engineering, University of Michigan-Dearborn, Dearborn, Michigan; [3]Department of Biological Sciences, Louisiana State University, Baton Rouge, Louisiana; and [4]Department of Mechanical Engineering, University of Minnesota, Minneapolis, Minnesota

ABSTRACT   Long-term storage of desiccated nucleated mammalian cells at ambient temperature may be accomplished in a stable glassy state, which can be achieved by removal of water from the biological sample in the presence of glass-forming agents including trehalose. The stability of the glass may be compromised due to a nonuniform distribution of residual water and trehalose within and around the desiccated cells. Thus, quantification of water and trehalose contents at the single-cell level is critical for predicting the glass formation and stability for dry storage. Using Raman microspectroscopy, we estimated the trehalose and residual water contents in the microenvironment of spin-dried cells. Individual cells with or without intracellular trehalose were embedded in a solid thin layer of extracellular trehalose after spin-drying. We found strong evidence suggesting that the residual water was bound at a 2:1 water/trehalose molar ratio in both the extracellular and intracellular milieus. Other than the water associated with trehalose, we did not find any more residual water in the spin-dried sample, intra- or extracellularly. The extracellular trehalose film exhibited characteristics of an amorphous state with a glass transition temperature of ~22°C. The intracellular milieu also dried to levels suitable for glass formation at room temperature. These findings demonstrate a method for quantification of water and trehalose in desiccated specimens using confocal Raman microspectroscopy. This approach has broad use in desiccation studies to carefully investigate the relationship of water and trehalose content and distribution with the tolerance to drying in mammalian cells.

INTRODUCTION

Lyopreservation, the storage of biologics in a desiccated state at ambient temperature, is a simple and cost-effective biobanking method that is an attractive alternative to cryopreservation (1–3). It has the potential to facilitate the broad dissemination of emerging technologies such as cellular and regenerative therapies (4–6), cell-based diagnostic assays, and biosensors (7,8). The idea of dry storage of mammalian cells stems from the discovery of the naturally evolved protection strategies in anhydrobiotic organisms, which include bacteria, yeast, nematodes, rotifers, tardigrades, certain crustaceans, and an insect, to survive hostile conditions including extreme heat and drought (9,10). A common protection strategy among anhydrobiotic organisms is the intracellular synthesis and accumulation of several osmolytes, including the disaccharide trehalose (11,12). The exact mechanism by which trehalose offers protection against desiccation has attracted a significant amount of interest. The early studies on the protective action of trehalose suggested that trehalose maintained the membrane in a liquid

crystalline state by substituting water through interacting with membrane hydrophilic headgroups, which is referred to as the water replacement hypothesis (13,14). Alternatively, glass formation hypothesis suggests that upon removal of water, the sugars assist in the formation of an intracellular glass with extremely high viscosity that hinders the molecular motion and decreases residual water mobility (15,16). The latter describes how trehalose contributes to the stability of intracellular milieu, whereas the former explains the beneficial direct interaction of trehalose with cellular membranes and structures. Another hypothesis, namely water entrapment, suggests that at low water contents, trehalose entraps residual water at the protein-sugar interface by glass formation, thereby preserving the structure of the proteins as well as membranes (17). These hypotheses are not necessarily mutually exclusive, but rather complementary in describing the protective action of trehalose in biological systems.

In recent years, the lyopreservation field has advanced in many fronts including understanding of the protective mechanisms of trehalose, the techniques for loading of trehalose into mammalian cells, and improved desiccation methods. Nonetheless, the successful desiccation and long-term storage of mammalian cells at ambient temperature is yet to be achieved, with the most notable exception being the dried storage of anucleated platelets (1,19–24).

It is suggested that spatial heterogeneity and incomplete desiccation is a potential reason for the failure of cell desiccation attempts (25–29). Desiccation of cells in sessile droplets, as performed in most studies, is prone to formation of a glassy skin at the air-liquid interface. The glassy skin reduces the drying rate and causes significant heterogeneities in the water and trehalose distributions within the drying sample (28). More recently, we developed a spin-drying technique for uniform and rapid desiccation of attached nucleated mammalian cells (30). However, there is no information available at single-cell level yet on how the intracellular trehalose may affect the drying of the intracellular milieu after spin-drying. Therefore, a detailed examination and quantification of water and trehalose at the single-cell level in spin-dried samples is needed to identify any potential heterogeneity that could cause instability of the intracellular glass.

Spectroscopic methods are extensively used for studying protein-water-trehalose interactions in mixtures, liposomes, and cells (17,31–34). Because of its label-free detection capabilities, Raman spectroscopy has recently been used in studying biological cells (35). In this study, we used confocal Raman microspectroscopy to measure water content in desiccated cells. First, we describe a characterization technique for the application of Raman microspectroscopy to estimate the water content in drying samples. Our characterization technique reintroduces Raman microspectroscopy as a useful technique for measurement of residual water, to the field of lyopreservation where accurate measurement of residual water is of interest. We then apply this technique to resolve the water content and distribution in our spin-dried samples at a single-cell level. Our findings suggest that, spin-drying of cell monolayers under saturated trehalose solution resulted in a small amount of residual water with a 2:1 water/trehalose molar ratio (0.05 g/g dry weight) in both the intra- and extracellular milieus. Such low intracellular water content could facilitate glass formation at room temperature by intracellular proteins. In the extracellular milieu, we found direct evidence of amorphous trehalose formation. We also found strong evidence that trehalose intracellular presence reduced desiccation-induced conformational changes in proteins. In this study, we introduce a method for simultaneous measurement of water and trehalose in spin-dried samples using Raman microspectroscopy. We envision that this method can be easily adapted in cell desiccation studies to accurately measure water and trehalose contents and to examine the state of intra/extracellular milieus as well as protein-trehalose interactions and conformational changes, which are the key factors for assessment of the efficacy of lyopreservation strategies.

MATERIALS AND METHODS

HepG2-TRET1 (36), a genetically modified line of human hepatoma cell line, HepG2-C3A (ATCC, Manassas, VA) cells were used in this study.

The HepG2-TRET1 line is genetically modified to express trehalose transporter membrane proteins to allow intracellular loading of extracellular trehalose. The HepG2-C3A cells were used as the control group. We will refer to these two cell lines as TRET and C3A, respectively, for the sake of brevity.

Cell culture

TRET and C3A cells were grown to 70–90% confluence in 75 cm^2 tissue culture-treated flasks (Corning, Sigma-Aldrich, St. Louis, MO) with Dulbecco's modified Eagle medium (DMEM, Invitrogen, Life Technologies, Grand Island, NY), supplemented with filtered heat-inactivated fetal bovine serum, at 37°C with 5% CO_2. Phosphate buffered saline solution (PBS) was prepared by dissolving 1 PBS tablet (Sigma-Aldrich) in 200 ml distilled water and sterile-filtering using a 0.2 μm bottle-top vacuum filter (Corning, Sigma-Aldrich).

Trehalose-cell lysate samples

At least 10^7 C3A cells were washed twice by pelleting and resuspending in PBS. The cells were lysed after the removal of supernatant in the last step by resuspending in distilled water. The suspension was freeze-thawed thrice by alternating between liquid nitrogen and a 37°C bath. The cell lysate was then homogenized by sonicating 3 times for 10 s using a Branson Sonifier 450 (VWR, Radnor, PA). The cell lysate was then filtered using a 0.2 μm Nalgene syringe filter (ThermoScientific, Waltham, MA). To obtain the dry mass of the cell suspension, a volume of the cell lysate was carefully weighed before and after drying overnight in the oven at 70°C. For complete removal of water, and also to reduce the degradation of biological matter, 70°C was found suitable (37,38). To make trehalose-cell lysate mixtures at known weight ratios, trehalose was weighed and added to the cell lysate solution at 1:1, 2:1, 4:1, and 10:1 mass ratios. Small volumes of cell lysate-trehalose mixtures were smeared on a clean, dry CaF_2 disk. Raman spectra of the drying layer were collected at intervals and the weight was recorded before and after each acquisition for calculation of water loss. Finally, the samples were placed in a 70°C oven overnight to allow for evaporation of any residual water (higher temperatures were avoided to reduce the degradation of biological matter). Weight loss was then recorded and the final spectrum was collected from each sample in the same manner.

Cell sample preparation

Forty-eight hours before the experiment, the cells were detached from the flask by incubating with 5 ml of 10× diluted 0.5% Trypsin-EDTA (Gibco, Life Technologies, Grand Island, NY) in PBS for 5 min. Trypsin was then neutralized by adding an equal volume of DMEM and the cells were pelleted by centrifuging at 750 × g for 5 min. After aspirating the supernatant, cells were resuspended in DMEM and were seeded on clean CaF_2 disks (Thor Labs, Newton, NJ) at a density of 2 × 10^5 cell/disk. CaF_2 disks were chosen to reduce the background fluorescence that is a problem with regular glass disks. The cells were allowed to attach for 2 h before replacing the medium with fresh DMEM. Similar steps were followed for TRET cells, except that in the last step, the media was replaced with DMEM containing 100 mM trehalose (Ferro-Pfanstiehl, Waukegan, IL) after 24 h.

Spin-drying experiments

The desiccation medium containing 1.8 M trehalose (Ferro-Pfanstiehl), 10 mM KCl (Sigma-Aldrich), 5 mM glucose (Sigma-Aldrich), 20 mM HEPES (Sigma-Aldrich), and 120 mM choline chloride (Sigma-Aldrich) was prepared. Spin-drying was performed using a commercially available spinning machine (model Cee 200, Brewer Science, Rolla, MO) as

described previously (22). Before spin-drying, the cell monolayer grown on the disks was washed with PBS. PBS was then removed and an excess amount of desiccation medium was added to cover the cells. The nitrogen flow was adjusted using a gas flow meter to provide an inert environment above the disk. At this point, the disks were spun at 1000 rpm for 60 s. After spinning, the samples were immediately transferred to plastic bags, vacuum-packed, and sealed. The disks were then transferred to the confocal Raman microscope and the spectra were collected within 4 h of the experiments.

Raman spectroscopy setup

A WITEC Alpha-300 system (WITEC, Ulm, Germany) with confocal capabilities with a 532 nm Ar-ion laser with 15 mW of power was used for excitation of samples. Single spectra from trehalose-cell lysate mixtures collected at 50–100 times with 0.1 s integration times. For cell samples, spectrum collection and integration time was set to 1 and 0.5 s, respectively. A cross section of the desiccated cell monolayers of C3A and TRET cells and the surrounding were scanned confocally starting a few microns over the cell (in the air) down to a few microns below the monolayer (within the CaF_2 disk). The theoretical confocal resolution of the microscope was set to ~200 nm in the XZ plane, as a result of an optic fiber cable with inner diameter of 50 μm, which collected and directed the scattered Raman photons to a DV401 charged-coupled device detector (WITEC) cooled down to $-60°C$ with 600/mm grating and 3 cm^{-1} spectral resolution. The laser light was directed to the samples placed on a controlled motorized stage using a 100× air objective (NA = 0.90; Nikon Instruments, Melville, NY) and a maximum theoretical resolution of ~1 μm in the XY plane.

Spectral analysis and calibration

Savitzky-Golay smoothing and background subtraction were performed on the collected spectra using WITEC Project software (version 2.10). The analysis was performed based on magnitude and location of the peaks of interest, as the following: All the peak assignments in this article are based on (39,40) listed in Table 1, unless otherwise mentioned. In the C3A and TRET cell samples, for comparing the intracellular and extracellular trehalose and water contents, the collected spectra were spatially averaged over representative volumes (see the Supporting Material Fig. S1).

To compare the average water and trehalose contents between samples, the spectral intensities collected from the samples were normalized to the protein peak at 1667 cm^{-1}. The contribution of water to the protein peak at 1667 cm^{-1} was accounted for by calibrating the intensity ratio of protein to total organic matter (I_{1667}/I_{2940}) against water content, which was measured gravimetrically. To calibrate for trehalose, spectra from spin-dried trehalose (dissolved in distilled water), homogenized cell lysate, and mixtures of known weight ratios of cell lysate to trehalose (LYS/TRE ratios of 1:0, 1:1, 1:2, 1:4, and 1:10) were collected separately, and

the ratio of I_{851}/I_{1667} was calculated for each LYS/TRE ratio. In the analysis of the water spectra, the peaks at 3300 cm^{-1} and 3430 cm^{-1} were considered to represent water in bound and free states, respectively (41). The contributions of proteins and trehalose to the selected peaks for water were dissociated by calibrating the intensity ratios of water peaks to total organic matter (I_{3300}/I_{2940} and I_{3430}/I_{2940}) against water content. For constructing confocal Raman images of the cells embedded in the trehalose layer, the intensity of the trehalose peak was corrected for the baseline induced by intracellular matter, and an intensity heat map was produced using the WITEC Project software.

RESULTS

Trehalose and water in dried cell lysate

The spectrum of dried homogenized cell lysate was obtained from C3A cells (Fig. 1 a). The C-H vibration from amino acids such as cytosine, guanine, tyrosine, and phenylalanine (1170–1185 cm^{-1}), $C-H_2$ deformation vibrations (1437–1453 cm^{-1}), and the Amide I band (1630–1680 cm^{-1}) were identified in the dried cell spectrum. Water bending vibration gives rise to a peak at ~1645 cm^{-1}, which contributes to the Amide I band region. Furthermore, other less strong but significant peaks could be observed at 754 cm^{-1}, 790 cm^{-1}, and 1009 cm^{-1}, attributed to cytochrome c (42), tryptophan (39), DNA and RNA (39), and phenylalanine (39), respectively. The C-H stretch peak in 2800–3000 cm^{-1} is the most intense peak observed in the cell lysate spectrum representing all the organic matter in the sample.

Upon addition of trehalose to the cell lysate mixture, distinct trehalose peaks at 485, 536, 851, 920, 1130, 1360, and 1465 cm^{-1} were observed in the fingerprint region of the spectra. These peaks increased in intensity with the decrease in the LYS/TRE ratio at 1:1, 1:2, 1:4, and 1:10. A C-H vibration peak originating from trehalose also became more pronounced at 2910 cm^{-1}. Trehalose peaks in the fingerprint region (400–1800 cm^{-1}) partially overlap with the various peaks originating from the cells. The range from 840 to 860 cm^{-1} is one of the most notable regions where saccharides (mono-, di-, and poly-) exhibit distinct and sharp Raman peaks due to resonance vibration from C-O-C skeletal structure and C-C bond stretching. As cells

TABLE 1   Selection of wavenumbers representing various vibrations of interest from trehalose, water, and proteins

| Component	Frequency (cm^{-1})	Ref.	Selected for this study
Trehalose	407, 528, 838, 912, 1120, 1149, and 1358 (only very strong peaks are reported)	(40)	851 cm^{-1} (C–O–C skeletal mode representing mono-, di-, and polysaccharides) for quantification of trehalose
Proteins	1637 – α-helix and β-structure of Amide I 1650 – C=C Amide I 1667 – C=C stretching band 1685 – Amide I (disordered structure; nonhydrogen bonded)	(39)	1667 cm^{-1} for quantification of the protein and lipid content
Organic material	2900–2915 – C-H stretch of lipids, proteins, and carbohydrates including disaccharides	(39)	2940 cm^{-1} for quantification of total organic matter including trehalose
Water	~3250 – O-H symmetric stretch (weak shoulder) low energy – more structured	(41)	3300 cm^{-1} for bound water
	~3430 – O-H antisymmetric stretch (strong shoulder) weakly bound high energy – loosely structured		3430 cm^{-1} for free water
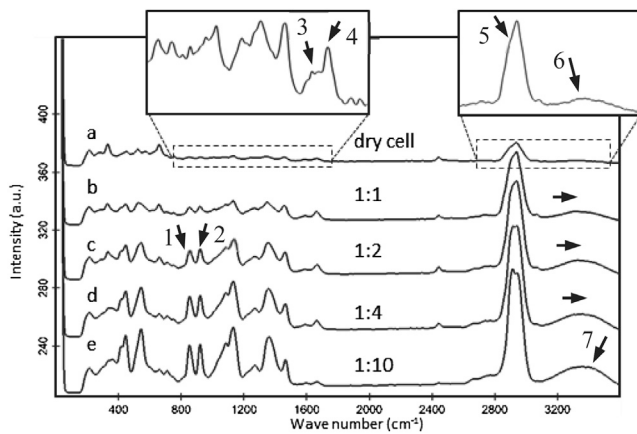
FIGURE 1 Raman scattering spectra collected from (*a*) dry cell lysate, (*b–e*) mixtures of cell lysate/trehalose at ratios of 1:1, 1:2, 1:4, and 1:10 g trehalose/g dry weight. Inset: blow-up of the region 720–1800 cm^{-1}. Annotations – 1), 851 cm^{-1} (saccharides, trehalose), 2), 920 cm^{-1} (C-C stretch of saccharides), 3), 1583 cm^{-1} (attributed to C=C stretch in L-tryptophan, various nucleic acids, guanine, phenylalanine), 4), 1667 cm^{-1} (protein band, Amide I), 5), ~2940 cm^{-1} (C-H stretch of organic matter), 6), 3250–3350 cm^{-1} (O–H symmetric stretch low energy band), 7), 3350–3500 cm^{-1} (O–H antisymmetric stretch high energy band).

normally contain simple sugars, a peak at ~851 cm^{-1} can be identified in cell lysate spectrum as well.

In the 2800–3000 cm^{-1} region, the strong peaks arising from C-H, C-H$_2$, and C-H$_3$, identifying all the organic material including trehalose, are distinct in all ratios of LYS/TRE. With increasing concentration of trehalose, the C-H bond shoulder at 2910 cm^{-1} becomes more pronounced compared to the peak at 2940 cm^{-1}. In 3100–3600 cm^{-1}

(O-H stretch) region, the presence of O-H groups in proteins and possibly the water in their hydration layers give rise to a weak peak at ~3300 cm^{-1} with an asymmetric, wide base spanning the 3100–3600 cm^{-1} range. In aqueous solutions, the O-H stretch peak is significantly large and wide with two distinct shoulders at ~3250 cm^{-1} and ~3430 cm^{-1} (43). A noticeable difference is observed in the shape of the O-H stretch peak when trehalose is added to the cell lysate mix. With increasing ratio of LYS/TRE, the broad peak in the O-H stretch region becomes wider, gets uniformly distributed and increases in intensity with the center of the broad peak moving toward ~3400 cm^{-1}.

Spectral overlap of water, trehalose, and proteins

The intensity of water bending vibration at ~1645 cm^{-1} is ~20 times less than the O-H stretch vibration in 3000–3600 cm^{-1} region; however, it overlaps with the Amide I peak at 1667 cm^{-1}. Analysis of the results in control samples indicated that, regardless of the LYS/TRE ratio, the normalized intensity of Amide I peak (I_{1667}/I_{2940}) converges toward a constant value upon removal of water from the solution, suggesting that the contribution of water bending vibration peak to the Amide I band might be negligible at low water contents (≤ 0.1 g water/g dry weight). The water content of the nitrogen and oven-dried samples (the data points along the dashed line) increases with increasing concentration of trehalose (Fig. 2 *A*), confirming the strong water affinity of trehalose (44). Note that oven-drying (the data points at 0 g$_{water}$/g$_{dry-weight}$) does not significantly decrease the I_{1667}/I_{2940} ratio when compared to convective
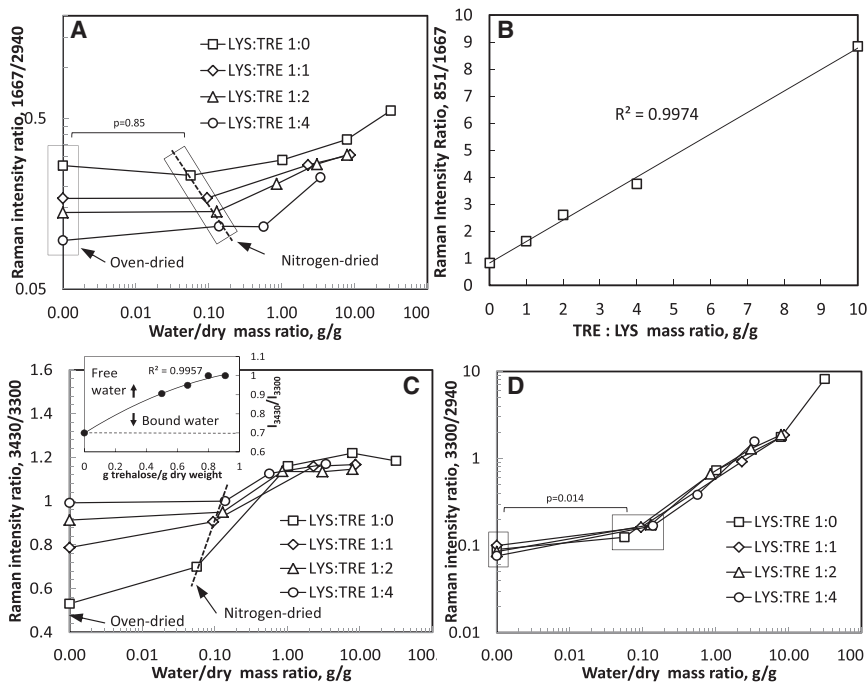

FIGURE 2 (*A*) Ratio of the Raman intensity of the peak at 1667 cm^{-1}, representing proteins, to the C-H stretch peak intensity at 2940 cm^{-1}, representing all the organic matter, at various LYS/TRE ratios against water content. (*B*) Calibration curve for (trehalose/protein) ratio based on intensity ratio of 851 cm^{-1} to 1667 cm^{-1} in oven-dried (0 g water/g dry weight) samples. (*C*) Ratio of O-H stretch intensities at 3430 cm^{-1} to 3300 cm^{-1} at various LYS/TRE ratios against water content (*Inset*: The intensity ratio 3430 cm^{-1} to 3300 cm^{-1} for nitrogen-dried samples plotted against TRE/LYS ratios. *Dashed line* denotes the background intensity not from water). (*D*) Ratio of the O-H stretch intensity at 3430 cm^{-1} to that of C-H stretch at 2940 cm^{-1} at various LYS/TRE ratios against water content.

drying with nitrogen ($p = 0.85$). This observation shows that, in extensively dried samples, the peak at 1667 cm^{-1} can be used to quantify the intracellular organic matter content.

The intensity ratio of a pronounced trehalose peak at 851 cm^{-1} to a protein peak at 1667 cm^{-1} (I_{851}/I_{1667}) is used to calibrate the trehalose content in the samples. This ratio is calculated and plotted versus the LYS/TRE ratio in Fig. 2 B. The intensity ratio I_{851}/I_{1667} linearly increases with the LYS/TRE ratio ($R^2 = 0.997$). The intercept of the linear fit to the data in Fig. 2 B corresponds to the background signal from intracellular mass. Various intracellular components including glycogens give rise to peak intensities at similar wavenumbers to trehalose (39), causing the background in Fig. 2 B.

Peak deconvolution of the O-H stretch region for wet samples resulted in the same two major peaks at ~3250 cm^{-1} and ~3430 cm^{-1} as suggested in other studies (41,43), representing low-energy bound water and high energy free water, respectively. Peak deconvolution in the spectra of dried samples also suggested presence of multiple peaks due to proteins with a major peak at ~3300 cm^{-1} (results not shown). Therefore, to calibrate the O-H stretch region for contributions of bound and free water, trehalose and proteins, O-H stretch intensity at 3300 cm^{-1} and 3430 cm^{-1} were selected for the analysis. In Fig. 2 C, the ratio I_{3430}/I_{3300} is plotted against water content for different LYS/TRE ratios. At high water contents (>1 g water/g dry weight), the ratio I_{3430}/I_{3300} remains between ~1.1–1.2 regardless of LYS/TRE ratio. When water is removed from the samples, the ratio I_{3430}/I_{3300} drops significantly. In the sample without trehalose, the I_{3430}/I_{3300} ratio dropped to 0.53 for 0 g water/gr dry weight (oven-dried cell lysate sample). With the addition of trehalose, the I_{3430}/I_{3300} ratio at 0 g water/ g dry weight increases, which is due to the contribution of trehalose to the O-H stretch region at ~3430 cm^{-1}. This shows the importance of proper calibration of the peak intensities in the O-H stretch region for water content measurement. To dissociate between free and bound water, we assumed that all the water retained in the sample after spin-drying was bound water, which could be removed by oven-drying. In the inset in Fig. 2 C, I_{3430}/I_{3300} intensity ratio is plotted against total dry weight for the nitrogen-dried samples. With no trehalose present (i.e., dried protein only), I_{3430}/I_{3300} had a background value of ~0.7. With increasing amount of trehalose, I_{3430}/I_{3300} increased and plateaued at 1. The line denoted by these data points may be used to dissociate between free and bound water for a given trehalose/protein weight ratio.

An interesting observation is made when the ratio I_{3300}/I_{2940} is plotted against the water content. In Fig. 2 D, regardless of the LYS/TRE ratio, the I_{3300}/I_{2940} ratio changes only with water content. This can be due to equal contribution of trehalose to both of the vibrational bands at 2940 cm^{-1} and

3300 cm^{-1}. Therefore, the amount of trehalose in samples does not affect the I_{3300}/I_{2940} ratio. At water contents below 0.1 g/g dry weight, the difference between the I_{3300}/I_{2940} ratio for the oven-dried and nitrogen dried groups, though small, is statistically significant ($p = 0.014$). This allows for dissociating the contribution of water from proteins and trehalose and calibration of water content based on the I_{3300}/I_{2940} ratio.

Trehalose and water content: C3A vs. TRET

We next probed into the microenvironment of the desiccated cells to measure the distribution of water and trehalose. Fig. 3, A1 and A2, show the brightfield images of C3A and TRET cells, respectively, in the XY plane (observed from above), embedded underneath dried trehalose layer. The presence of trehalose coating distorts the light at boundaries of the cell, which creates contrast for imaging. In Fig. 3 B, spatially averaged spectra from intracellular regions of the C3A and TRET cells are presented. The area-averaged spectrum from each cell was normalized to its maximum spectral intensity. Area averaging was performed over the intra- and extracellular milieus (Fig. S1), with the XZ planes (top to bottom) represented by the black dotted lines in Figs. 3, A1 and A2.
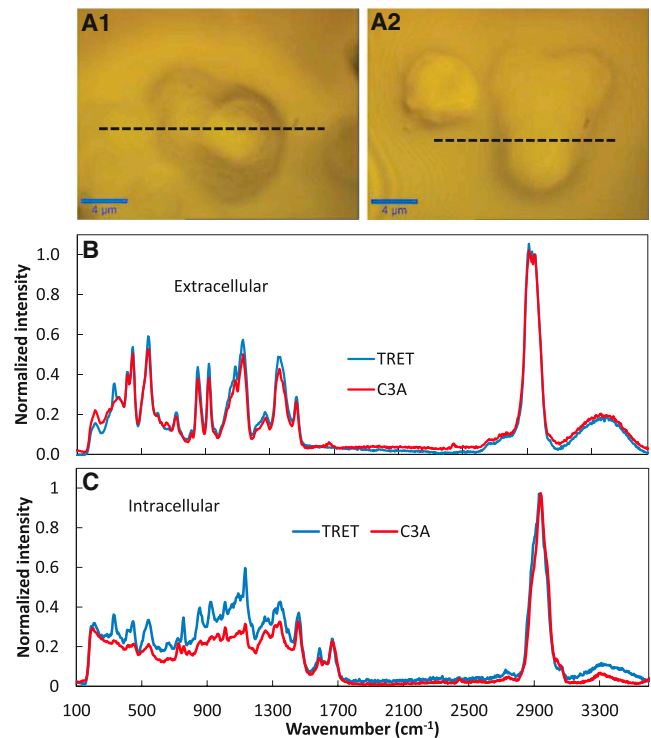

FIGURE 3 (A1 and A2) Brightfield images of C3A and TRET cells, embedded in a trehalose layer after spin-coating and desiccation under nitrogen flow. The white dotted line represents the XZ plane of scan. (B) Area-averaged intracellular spectrum collected from C3A and TRET cells. (C) Area-averaged spectra collected from the extracellular thin layer of trehalose.

The averaged intracellular spectra from the C3A and TRET cells showed significant differences in the 400–1800 cm^{-1} region. Generally, the intensity of the TRET spectrum was higher than that of the C3A after background subtraction (Fig. 3 B). This increased intensity could be attributed to the presence of intracellular trehalose in the TRET cell. Quantitative analysis of trehalose content in cells was performed based on the normalized intensities of I_{851}/I_{1667}. The results suggest an average value of 0 and 0.7 g trehalose/g protein for C3A and TRET cells, respectively, based on calibration data in Fig. 2 B.

In the 3100–3600 cm^{-1} region, the hydroxyl vibration intensity is very weak in both cells, with a wide peak at 3300 cm^{-1}. Quantitative analysis of water content was done based on the I_{3430}/I_{3300} and I_{3300}/I_{2940} ratios in Fig. 3 B according to calibration presented in Fig. 2, C and D, respectively. For the C3A and TRET cells, I_{3300}/I_{2940} ratios were similar and corresponded to ~0 and ~0.05 g water/g dry mass. The I_{3430}/I_{3300} ratios were 0.7 and 0.85, respectively, suggesting no free water in either cell (Fig. 2 C, inset). The measurements were performed on the collective average from many cells in each group (Fig. S2). The estimations for water and trehalose contents in the TRET cells suggest that water/trehalose mass ratio is ~0.12. This value is ~2 water molecules per trehalose molecule. The spectra collected from the extracellular regions of both cell types, plotted in Fig. 3 C, display the entire characteristic peaks of trehalose including those at 528, 851, 920 cm^{-1}. The peaks in the 1500–1700 cm^{-1} region, representing the proteins, are absent in the extracellular spectra as the extracellular region contains only trehalose and small concentrations of other solutes as mentioned in the Methods section. Trehalose peaks observed in the fingerprint region resemble the Raman spectral characteristics of amorphous trehalose (38). The shape and intensity of the hydroxyl stretch vibration (3100–3600 cm^{-1}) in the extracellular region are identical in shape in both samples, exhibiting a symmetric distribution, and are significantly different from those of the intracellular region. The I_{3300}/I_{2940} ratios are 0.18 in the extracellular milieu of the C3A and TRET cells, corresponding to ~0.11 g water/g dry weight, which is equivalent of ~2 water molecules per trehalose molecule. The I_{3430}/I_{3300} ratio is equal to 1, which suggests the residual water is bound (Fig. 2 C, inset). It must be mentioned that the other small solutes in the desiccation medium sum up to <4% w/w of total dried thin layer, and were considered in this calculation. A summary of our findings are presented in Table 2.

Intracellular distribution of water and trehalose: C3A vs. TRET

To investigate the potential drying-induced heterogeneities within and in the vicinity of the desiccated cells, we reconstructed images of cells based on protein, trehalose, and

TABLE 2 Summary of results on the overall distribution and state of water and trehalose in C3A and TRET cells

	C3A		TRET	
	Intracellular	Extracellular	Intracellular	Extracellular
Water content (g/g dry weight)	0.00	0.11	0.05	0.11
State of water	–	Bound	Bound	Bound
Trehalose content (g/g dry weight)	0.00	0.97[a]	0.41[b]	0.97[a]
Water/trehalose molar ratio	–	2:1	2:1	2:1

[a]3% w/w other salts in the drying medium.
[b]TRET intracellular trehalose content: 0.7 g/g protein ≈ 0.41 g/g dry weight.

O-H stretch distributions as presented in Fig. 4, with C3A and TRET cells presented in column A B, respectively. In column C, the distributions of protein, trehalose, and O-H stretch are plotted across the width of the cell. In Fig. 4, A1 and B1, the protein contrast images identify the cell presence and boundaries. The overall shape of the C3A cell appears flattened with rough edges as opposed to the TRET cell which looks round with smooth edges. The distribution of protein in the C3A cell shows large variations across the cell width with peaks showing local concentration of proteins. On the other hand, the distribution of protein in the TRET cell smoothly transitions from one end to the other with minimal variation (Fig. 4 C1). This phenomenon was observed in many cells in each group (Fig. S3) and suggests that the intracellular trehalose contributed to a more uniform distribution of intracellular proteins in cells when water was removed.

In the trehalose-contrast image in Fig. 4 A2, a high extracellular concentration of trehalose results in a sharp contrast between the intra- and extracellular milieu for the C3A cell. This contrast is less sharp in Fig. 4 B2 for the TRET cell where we expect intracellular presence of trehalose. This difference can be seen clearly in Fig. 4 C2, where trehalose intensity falls sharply in both cells at cell boundaries and reaches ~0 in the C3A cell, but it remains at about one-third of the extracellular intensity in the TRET cell. Trehalose distribution within the cell was quantified by calculating I_{851}/I_{1667} ratio across the cell width using the calibration data in Fig. 2 B. It must be noted that I_{851}/I_{1667} cannot be calculated outside the cell. Therefore, only the region containing the cell is plotted in Fig. 4 D. For the C3A cell, trehalose content decreased sharply to ~0 g trehalose/g dry mass and remains approximately uniform across the cell width (Fig. 4 D). In the TRET cell, trehalose content gradually decreases from values as high as ~1–1.5 g trehalose/g protein at cell boundaries to ~0.2 g trehalose/g protein in the middle of the cell. This also suggests that trehalose may not be evenly distributed across the cell width. Incidentally, the region with highest protein content contains the lowest trehalose content.
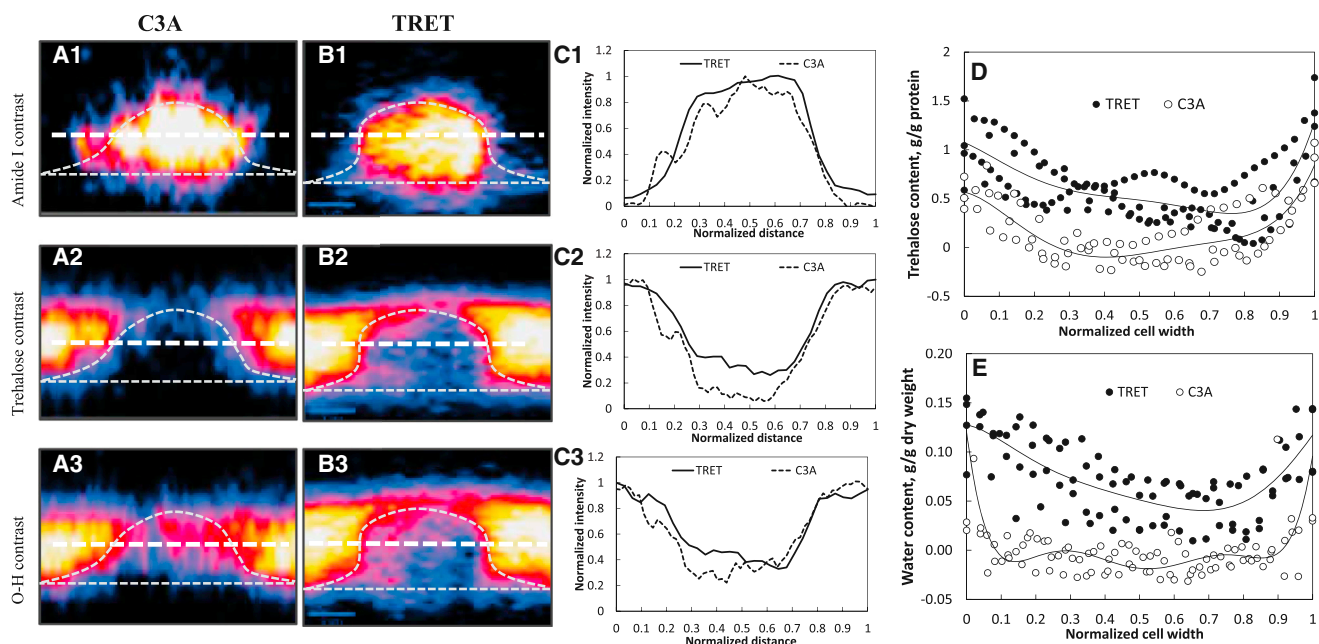
FIGURE 4 Reconstructed confocal Raman images of C3A (*A1–A3*) and TRET (*B1–B3*) cells, based on protein (*row* 1), trehalose (*row* 2), and O-H stretch (*row* 3) contrasts. Images show cross sections of cells in the XZ plane, with air at the top and CaF$_2$ substrate at the bottom. The thin gray lines constitute the approximate boundaries of the cells (*C1–C3*) Respective distributions of proteins, trehalose, and O-H stretch across the cell width along the thick dashed white line. (*D* and *E*) Estimated amount of trehalose/protein and water/dry weight ratios from I_{851}/I_{1667} and I_{3300}/I_{2940} ratios, respectively.

To identify water presence, the distribution of O-H stretch across the cell thickness in C3A and TRET cells were compared as presented in Fig. 4, *C1* and *C2*, respectively. The images were reconstructed based on the area under the peak of O-H stretch in the 3100–3600 cm^{-1} region. Water, trehalose, and proteins all contribute to the O-H stretch region of the Raman spectrum. To estimate water content, I_{3300}/I_{2940} intensity ratio were calculated across the cell width. With no trehalose present, the O-H stretch distribution in the C3A cell varied at values around 0 g water/g dry weight (Fig. 4 *E*). For the TRET cell, O-H stretch distribution closely followed that of trehalose, decreasing from 0.12 to 0.05 on average (Fig. 4 *E*). Hence, a small amount of water retained in the TRET cells, possibly due to the presence of a significant amount of intracellular trehalose.

Based on the results presented in Figs. 3 and 4, water and trehalose distribution in the extracellular bulk of the cell appeared uniform and sharply decreased at the cell boundaries. In both intra- and extracellular milieu, we observed no free water retention. Trehalose, at the levels loaded into TRET cells in this study (~0.7 g/g protein) resulted in a small increase in water retention. The residual water in both intra- and extracellular milieu was bound and correlated with trehalose content at ~2:1 molar ratio.

DISCUSSION

For successful storage of desiccated cells at room temperature, formation of intracellular glass is one of the essential requirements, which can typically be achieved at a low intracellular water content (<0.1 g/g dry weight) in a glass-forming liquid (45). Thus, in lyopreservation studies, careful measurement of the intracellular water content after desiccation is critical. Generally, the bulk water content of the sample is measured and it is assumed to be uniformly distributed throughout the desiccated sample. However, the difference in the composition of intra- and extracellular milieus may lead to different drying kinetics, resulting in variations in respective final water contents after desiccation. This difference may be augmented in the presence of lyoprotective agents such as trehalose. Therefore, methods for careful measurement of both intracellular water and trehalose are critical for the development of efficient desiccation protocols. We employed confocal Raman microspectroscopy to resolve the differences in water and trehalose contents between intra- and extracellular milieus. We correlated the measured water content with Raman peak intensity ratios for protein, trehalose, and water to produce calibration curves. We then examined spin-dried cells and their immediate microenvironment by Raman microspectroscopy, and used the calibration curves to estimate the water and trehalose content in the desiccated specimen. We employed the TRET cells with the enhanced ability to be loaded by trehalose. The C3A cells that lacked such ability were used as the control group. Because both cell types were desiccated under the same medium with similar spin-drying conditions, the extracellular milieu in both groups were identical in composition. The intracellular milieu of C3A and TRET cells however were found to be different in terms of water and trehalose contents after spin-drying.

An interesting observation was that the C3A cells did not retain any intracellular water after spin-drying in a trehalose containing extracellular solution. In contrast, the presence of intracellular trehalose in spin-dried TRET cells resulted in an increase in intracellular water content at a water/trehalose ratio of 2:1. Our measurements showed that this residual water was bound. The same 2:1 molar ratio for trehalose and water was found in the extracellular milieu. However, we did not observe the distinct sharp Raman peaks associated with the formation of crystalline trehalose dihydrate in the intra- or extracellular milieus.

We also found that the intracellular distributions of water and trehalose in the TRET cells were heterogeneous, slightly increasing from the middle of the cell toward the cell membrane (Fig. 4, D and E). Normalization to cell protein content and partial overlap with the extracellular trehalose near the cell membrane may have contributed to the observed increase in the intracellular distributions of both water and trehalose. This observation is novel, to our knowledge, and requires further investigation because a heterogeneous intracellular distribution of water and trehalose can offset the protection against desiccation damage and decrease the longevity of storage. Examination of the cells at higher spatial and spectral resolutions may allow obtaining more detailed information on the subcellular distribution of water and trehalose. In contrast, we found that, in the extracellular milieu, the distributions of water and trehalose were homogeneous throughout the spin-dried specimen. We found similar results for the spin-dried extracellular thin film of trehalose without the embedded cells in our previous study using Fourier transform infrared spectroscopy (30).

Studies in plant anhydrobiosis suggest that proteins may form glass at room temperature at 0.1–0.12 g water/g dry weight (45). Such glass formation may be accomplished without the presence of trehalose and even in desiccation-sensitive species. The measured final intracellular water content in both C3A and TRET cells were <0.1 g/g dry weight (Table 2). Therefore, there is a good chance that the intracellular milieu of C3A cells formed glass at room temperature with such low water contents. In the TRET cells, the intracellular proteins supplemented by intracellular trehalose may form a glass with higher than room-temperature Tg based on the Gordon-Taylor equation (46). In the extracellular milieu, we found that the spectrum of extracellular trehalose film closely matched that of the amorphous trehalose in the fingerprint region (38,47). The wide Raman peaks indicate a broad distribution of chemical bond energies as a result of random distribution of molecules. Interestingly, this was also identical to the Raman signatures of trehalose in aqueous solution where no trehalose structure exists. Because the extracellular milieu contained only trehalose and residual amount of salts, at 0.11 g water/g dry weight, the Tg of the extracellular milieu was ~22°C (48). Therefore, we suggest that the extracellular trehalose was in a glassy state after spin-drying. Based on

these results, it is likely that both intra- and extracellular milieu of spin-dried cells form glass at room temperature. The determination of the Tg of the intracellular milieu after spin-drying will allow optimization of the storage temperature.

In desiccation-sensitive species such as mammalian cells, desiccation-induced damage including protein denaturation may occur before the glassy state is reached. The benefit of trehalose in biopreservation might be not only because it is a potent glass forming agent, but also a very efficient bio-stabilizer for preservation of protein structure (49). In the spectra of the intracellular milieu of C3A cells, we observed a shift in the position of Amide II peak and considerable broadening of Amide I peak (Fig. S4). Many spectroscopic studies have attributed these spectral changes to the alteration of protein secondary structure (50–53). In comparison, in the TRET cells, the positioning of Amid II peak was identical to the trehalose-cell lysate mixtures and hydrated proteins, suggesting minimal alteration to the protein secondary structure in the dry state.

CONCLUSION

Residual water content, along with glass-forming agents such as trehalose, are the key parameters contributing to the formation and stability of the intracellular glass at room temperature. Hence, accurate measurement of intracellular water and trehalose allows predicting the efficacy of lyopreservation. In this study, we developed a calibration technique for the measurement of intracellular water and trehalose in desiccated cells using Raman spectroscopy. We were able to show that both intra- and extracellular milieus of spin-dried trehalose-loaded cells were dry with only a small amount of residual water content at a water/trehalose ratio of 2:1 in both milieus. Also using Raman spectroscopy we were able to find evidence of glass formation in the extracellular milieu. For the intracellular milieu, based on the measured water content, glass formation was plausible. We also observed inhomogeneity in the intracellular distributions of water and trehalose in spin-dried cells, which warrants further investigation. Furthermore, using Raman spectroscopy, we were able to show that the intracellular presence of trehalose reduced desiccation-induced conformational changes in proteins. We propose that the method introduced in this study can be easily adapted in lyopreservation studies to determine the role of water and trehalose content and distribution on the stability of desiccated sample.

SUPPORTING MATERIAL

Four figures are available at http://www.biophysj.org/biophysj/supplemental/S0006-3495(14)01006-6.

REFERENCES

1. Wolkers, W. F., N. J. Walker, …, J. H. Crowe. 2001. Human platelets loaded with trehalose survive freeze-drying. *Cryobiology.* 42:79–87.

2. Ma, X., K. Jamil, …, A. E. Oliver. 2005. A small stress protein acts synergistically with trehalose to confer desiccation tolerance on mammalian cells. *Cryobiology.* 51:15–28.

3. Elmoazzen, H. Y., G. Y. Lee, …, J. D. Biggers. 2009. Further optimization of mouse spermatozoa evaporative drying techniques. *Cryobiology.* 59:113–115.

4. Sane, S. U., R. Wong, and C. C. Hsu. 2004. Raman spectroscopic characterization of drying-induced structural changes in a therapeutic antibody: correlating structural changes with long-term stability. *J. Pharm. Sci.* 93:1005–1018.

5. Jamil, K., J. H. Crowe, …, A. E. Oliver. 2005. Arbutin enhances recovery and osteogenic differentiation in dried and rehydrated human mesenchymal stem cells. *Cell Preserv. Technol.* 3:244–255.

6. Adler, M., and G. Lee. 1999. Stability and surface activity of lactate dehydrogenase in spray-dried trehalose. *J. Pharm. Sci.* 88:199–208.

7. Bloom, F. R., P. Price, …, M. Potts. 2001. Engineering mammalian cells for solid-state sensor applications. *Biosens. Bioelectron.* 16:603–608.

8. Oliver, A. E. 2012. Dry state preservation of nucleated cells: progress and challenges. *Biopreserv. Biobank.* 10:376–385.

9. Wolkers, W. F., F. Tablin, and J. H. Crowe. 2002. From anhydrobiosis to freeze-drying of eukaryotic cells. *Comp. Biochem. Physiol. A Mol. Integr. Physiol.* 131:535–543.

10. Hand, S. C., M. A. Menze, …, D. Moore. 2011. Expression of LEA proteins during water stress: not just for plants anymore. *Annu. Rev. Physiol.* 73:810–820.

11. Clegg, J. S. 2005. Desiccation tolerance in encysted embryos of the animal extremophile, artemia. *Integr. Comp. Biol.* 45:715–724.

12. Westh, P., and H. Ramløv. 1991. Trehalose accumulation in the tardigrade *Adorybiotus coronifer* during anhydrobiosis. *J. Exp. Zool.* 258:303–311.

13. Webb, S. J. 1965. Bound Water in Biological Integrity. Thomas, Springfield, IL.

14. Clegg, J. S., P. Seitz, …, C. F. Hazlewood. 1982. Cellular responses to extreme water loss: the water-replacement hypothesis. *Cryobiology.* 19:306–316.

15. Green, J. L., and C. A. Angell. 1989. Phase relations and vitrification in saccharide-water solutions and the trehalose anomaly. *J. Phys. Chem.* 93:2880–2882.

16. Crowe, J. H., J. F. Carpenter, and L. M. Crowe. 1998. The role of vitrification in anhydrobiosis. *Annu. Rev. Physiol.* 60:73–103.

17. Belton, P. S., and A. M. Gil. 1994. IR and Raman spectroscopic studies of the interaction of trehalose with hen egg white lysozyme. *Biopolymers.* 34:957–961.

18. Reference deleted in proof.

19. Wolkers, W. 2003. Temperature dependence of fluid phase endocytosis coincides with membrane properties of pig platelets. *Biochim. Biophys. Acta (BBA)- Biomembr.* 1612:154–163.

20. Elliott, G. D., X.-H. Liu, …, M. Toner. 2006. Trehalose uptake through P2X7 purinergic channels provides dehydration protection. *Cryobiology.* 52:114–127.

21. Kikawada, T., A. Saito, …, T. Okuda. 2007. Trehalose transporter 1, a facilitated and high-capacity trehalose transporter, allows exogenous trehalose uptake into cells. *Proc. Natl. Acad. Sci. USA.* 104:11585–11590.

22. Chakraborty, N., M. A. Menze, …, M. Toner. 2011. Cryopreservation of spin-dried mammalian cells. *PLoS ONE.* 6:e24916.

23. Shirakashi, R., C. M. Köstner, …, V. L. Sukhorukov. 2002. Intracellular delivery of trehalose into mammalian cells by electropermeabilization. *J. Membr. Biol.* 189:45–54.

24. Eroglu, A., M. Toner, and T. L. Toth. 2002. Beneficial effect of microinjected trehalose on the cryosurvival of human oocytes. *Fertil. Steril.* 77:152–158.

25. Adams, D. R., M. Toner, and R. Langer. 2008. Microflow and crack formation patterns in drying sessile droplets of liposomes suspended in trehalose solutions. *Langmuir.* 24:7688–7697.

26. Aksan, A., S. C. Morris, and M. Toner. 2005. Analysis of desiccation and vitrification characteristics of carbohydrate films by shear-wave resonators. *Langmuir.* 21:2847–2854.

27. Aksan, A., and M. Toner. 2004. Isothermal desiccation and vitrification kinetics of trehalose-dextran solutions. *Langmuir.* 20:5521–5529.

28. Aksan, A., D. Irimia, …, M. Toner. 2006. Desiccation kinetics of biopreservation solutions in microchannels. *J. Appl. Phys.* 99:2181280.

29. Ragoonanan, V., and A. Aksan. 2008. Heterogeneity in desiccated solutions: implications for biostabilization. *Biophys. J.* 94:2212–2227.

30. Chakraborty, N., A. Chang, …, M. Toner. 2011. A spin-drying technique for lyopreservation of mammalian cells. *Ann. Biomed. Eng.* 39:1582–1591.

31. Dong, J., J. Malsam, …, A. Aksan. 2010. Spatial distribution of the state of water in frozen mammalian cells. *Biophys. J.* 99:2453–2459.

32. Oldenhof, H., W. F. Wolkers, …, J. H. Crowe. 2006. Freezing and desiccation tolerance in the moss *Physcomitrella patens*: an in situ Fourier transform infrared spectroscopic study. *Biochim. Biophys. Acta.* 1760:1226–1234.

33. Malsam, J., and A. Aksan. 2009. Hydrogen bonding and kinetic/thermodynamic transitions of aqueous trehalose solutions at cryogenic temperatures. *J. Phys. Chem. B.* 113:6792–6799.

34. Crowe, J. H., B. J. Spargo, and L. M. Crowe. 1987. Preservation of dry liposomes does not require retention of residual water. *Proc. Natl. Acad. Sci. USA.* 84:1537–1540.

35. Diem, M., M. Miljković, …, N. Laver. 2012. Applications of infrared and Raman microspectroscopy of cells and tissue in medical diagnostics: present status and future promises. *Spectrosc. Int. J.* 27:463–496.

36. Li, S., N. Chakraborty, …, S. C. Hand. 2012. Late embryogenesis abundant proteins protect human hepatoma cells during acute desiccation. *Proc. Natl. Acad. Sci. USA.* 109:20859–20864.

37. Surana, R., A. Pyne, and R. Suryanarayanan. 2004. Effect of preparation method on physical properties of amorphous trehalose. *Pharm. Res.* 21:1167–1176.

38. Chakravarty, P., S. P. Bhardwaj, …, R. Suryanarayanan. 2009. Monitoring phase transformations in intact tablets of trehalose by FT-Raman spectroscopy. *AAPS PharmSciTech.* 10:1420–1426.

39. Movasaghi, Z., S. Rehman, and I. U. Rehman. 2007. Raman spectroscopy of biological tissues. *Appl. Spectrosc. Rev.* 42:493–541.

40. De Gelder, J., K. De Gussem, …, L. Moens. 2007. Reference database of Raman spectra of biological molecules. *J. Raman Spectrosc.* 38:1133–1147.

41. Kahan, T. F., J. P. Reid, and D. J. Donaldson. 2007. Spectroscopic probes of the quasi-liquid layer on ice. *J. Phys. Chem. A.* 111:11006–11012.

42. Okada, M., N. I. Smith, …, K. Fujita. 2012. Label-free Raman observation of cytochrome *c* dynamics during apoptosis. *Proc. Natl. Acad. Sci. USA.* 109:28–32.

43. Branca, C., S. Magazù, …, P. Migliardo. 1999. α,α-Trehalose-water solutions. 3. Vibrational dynamics studies by inelastic light scattering. *J. Phys. Chem. B.* 103:1347–1353.

44. Magazu, S., P. Migliardo, ..., M. T. Sciortino. 1997. α,α-Trehalose-water solutions. 1. Hydration phenomena and anomalies in the acoustic properties. *J. Phys. Chem. B.* 101:2348–2351.

45. Buitink, J., and O. Leprince. 2008. Intracellular glasses and seed survival in the dry state. *C. R. Biol.* 331:788–795.

46. Gordon, B. M., and J. S. Taylor. 1952. Ideal copolymers and the second-order transitions of synthetic rubbers. I. Non-crystalline copolymers. *J. Appl. Chem.* 2:493–500.

47. Brown, G. M., D. C. Rohrer, ..., R. Simpson. 1972. The crystal structure of α,α-trehalose dihydrate from three independent X-ray determinations. *Acta Crystallogr. B.* 28:3145–3158.

48. Chen, T., A. Fowler, and M. Toner. 2000. Literature review: supplemented phase diagram of the trehalose-water binary mixture. *Cryobiology.* 40:277–282.

49. Carpenter, J. F., and J. H. Crowe. 1989. An infrared spectroscopic study of the interactions of carbohydrates with dried proteins. *Biochemistry.* 28:3916–3922.

50. Kumar, V., V. K. Sharma, and D. S. Kalonia. 2009. In situ precipitation and vacuum drying of interferon alpha-2a: development of a single-step process for obtaining dry, stable protein formulation. *Int. J. Pharm.* 366:88–98.

51. Kocherbitov, V., J. Latynis, ..., G. Niaura. 2013. Hydration of lysozyme studied by Raman spectroscopy. *J. Phys. Chem. B.* 117:4981–4992.

52. Tolleter, D., D. K. Hincha, and D. Macherel. 2010. A mitochondrial late embryogenesis abundant protein stabilizes model membranes in the dry state. *Biochim. Biophys. Acta.* 1798:1926–1933.

53. Souillac, P. O., C. R. Middaugh, and J. H. Rytting. 2002. Investigation of protein/carbohydrate interactions in the dried state. 2. Diffuse reflectance FTIR studies. *Int. J. Pharm.* 235:207–218.